Journal of Molecular Structure 1304 (2024) 137635

Contents lists available at ScienceDirect

Journal of Molecular Structure

journal homepage: www.elsevier.com/locate/molstr

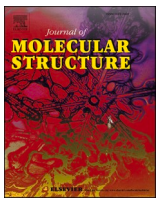

Synthesis and characterization of transparent phenothiazine-based polymers via Buchwald-Hartwig polymerization as promising functional organic materials

Mohamed M.H. Desoky [a], Federico Cruciani [a], Pierluigi Quagliotto [a,b,*], Guido Viscardi [a,b]

[a] Department of Chemistry, University of Torino, Via Pietro Giuria 7, Torino 10125, Italy
[b] NIS Interdepartmental Centre, University of Torino, Via Gioacchino Quarello 15/a, Torino 10135, Italy

ARTICLE INFO

Keywords:
Phenothiazine
Buchwald-Hartwig reaction
Polymers
DSC-TGA analysis
Optical properties

ABSTRACT

A novel series of polymers incorporating 10-hexyl-*10H*-phenothiazine and substituted anilines were synthesized through Buchwald-Hartwig amination polymerization. Comprehensive characterization of the polymers by Differential Scanning Calorimetry (DSC) and Thermogravimetric Analysis (TGA showed remarkable thermal stability. Size Exclusion Chromatography (SEC) measurements indicated low polydispersity, and average molecular weights, both conducive to film formation. Optical characterization, conducted through UV–vis absorption spectroscopy, highlighted the transparency of the synthesized polymers in the visible region. Additionally, band gap was estimated by the intersection point of absorption and emission spectra. This multifaceted analysis contributes valuable insights into the structural and optical properties of the developed polymeric compounds, demonstrating their potential applications in various fields.

1. Introduction

Recently, significant research attention has been devoted to transparent electronics for various technological advancements such as windscreen technology, smart windows, digital signage, smart glasses, and perovskite-based photovoltaics [1–4]. Transparent electronic devices offer the potential for transparent display systems with increased data output and compact sensing systems for enhanced information acquisition. The utilization of visible light communication (VLC) systems in vehicles, airplanes, and medical facilities has gained popularity due to their immunity to X-ray, ultraviolet (UV), and infrared (IR) interference [5–8]. However, transparent systems that detect visible light face a conflict between transparency and photodetector performance. Although UV and IR detection systems can circumvent this issue, they are incompatible with VLC systems that rely on light-emitting diodes (LEDs) as a light source and are unsuitable for large-area, low-temperature organic electronics intended for visible light detection [9–12]. To address this challenge, researchers have explored the integration of fine-grained inorganic materials such as nanoparticles or quantum dots with highly transparent oxide semiconductors [7,13–15]. Additionally, the development of extremely thin semiconductor layers holds promise for the fabrication of highly transparent visible-light phototransistors. However, excessively thin active layers tend to exhibit limitations such as low carrier mobility (μ), surface non-uniformity, and reduced drain current (ID) [12,16–19]. In light of these constraints, there has been a recent emphasis on the advancement of organic electronics. Organic electronics have gained attention due to their compatibility with low-cost, large-area, and low-temperature processing techniques enabled by the solution processing of small organic molecules and polymers [20,21]. In the field of perovskite-based photovoltaics, polymeric semiconductors provide holes transporting but also transparency that is essential to allow light to reach the active film and its protection from the humidity [22–24]. By employing rational material synthesis and molecular design, these materials can be tailored to enhance the performance of electronic devices through strategies such as doping and/or material mixing [25,26].

Successfully, we synthesized novel transparent polymers for organic electronics by employing Buchwald-Hartwig amination to combine N-alkyl phenothiazine and substituted anilines. The rationale behind the choice to use phenothiazine building block depends on the interesting properties of phenothiazine; firstly, the good electrochemical properties that justify their promising applications in material science as electron-donating units in electronically conducting charge-transfer materials [27]. They can also act as sensors in supramolecular systems for

* Corresponding author.
E-mail address: pierluigi.quagliotto@unito.it (P. Quagliotto).

https://doi.org/10.1016/j.molstruc.2024.137635
Received 30 June 2023; Received in revised form 8 January 2024; Accepted 23 January 2024
Available online 28 January 2024

photoinduced electron transfer (PET) [28–30]. Because of their low oxidation potential, phenothiazines are capable of acting as electron donors in fluorescent donor-acceptor chromophores, which are useful for organic light-emitting diode applications [31,32], and for electro-optical and nonlinear effect-based applications [33].

Furthermore, the phenothiazine is cheap, very stable, easy to alkylate on the nitrogen atom in order to tune solubility and its "butterfly" structure avoids packing and crystallization in the films used for different devices. All these characteristics make the phenothiazine an easy to manage and tunable scaffold for the building of functional organic materials. The triarylamine structure for the polymers was chosen since most polymers and small molecules used for organic electronic contains this motif structure. In fact, the introduction of triarylamines in functional materials for organic electronics is important since the nitrogen atom is involved in the electroactivity of the molecules/polymers, thus cooperating to the charge transport phenomena in the solid film normally used in device [34].

In recent years, the Buchwald-Hartwig cross-coupling has become a crucial tool in organic chemistry for the synthesis of carbon-nitrogen bonds via palladium-catalyzed cross-coupling reactions of aryl halides with amines [35]. This reaction has found widespread use in many fields, including pharmaceuticals, agrochemicals, natural products, and organic molecules related to material science. Numerous efforts have been made to develop better methodologies and catalysts for the Buchwald-Hartwig amination reaction in both academic research and industrial processes [36,37]. Compared to previous methods, such as nucleophilic aromatic substitutions (S_NAr) [38] or copper-mediated reactions [39], which have limitations such as a narrow substrate scope, long reaction times, and high temperatures, the Buchwald-Hartwig reaction is a more efficient method for the synthesis of carbon-nitrogen bonds. This reaction has also been applied to polymerizations, particularly in the synthesis of organic hole transport materials (HTMs) used in organic electronics. PTAA, a polymer belonging to the polytriarylamines class, is one of the most reliable and well-performing HTMs. The development of new, cheaper, and higher-performing HTMs has motivated researchers to develop better synthetic methods that can be adapted for polymerizations and to control the characteristics of the final product. Sprick et al. [40] demonstrated that the (NHC)-Pd catalyzed Buchwald amination polymerization of anilines and dibromoarenes can be used to prepare a library of PTAA-based molecules, and that adding fused ring structures into the polymer backbone and replacing the pendant phenyl groups with electron-withdrawing fluorine or electron-donating methoxy group can influence the molecular weight of the resulting polymer. Here, we are presenting a simple one-step polymerization method using a low-cost phenothiazine derivative and aniline derivatives and the characterization of the final polymers.

2. Experimental

2.1. Materials

All chemicals and solvents were purchased as pure grade for synthesis or spectroscopy from Merck, TCI Chemicals, abcr Gute Chemie and VWR, and used without further purification.

2.2. Instruments

2.2.1. NMR spectra

NMR spectra were recorded on a JEOL ECZ-R 600, working at 600 MHz and 151 MHz for ^{1}H and ^{13}C, respectively.

2.2.2. Mass spectra

MS spectra were performed using an Agilent-6890 GC, an Agilent-5973 Network mass selective detector, and an EI ionization system. The GC–MS was operated with an interface temperature of 300 °C and an ionization source temperature of 250 °C. A solvent delay of 4.0 min was set to protect the filament from oxidation. Chromatographic separation was achieved using Colum Agilent 19091S-433, HP-5MS, with nominal capillary of 30.0 m x 250 μm x 0.25 μm. Helium, with a minimum purity of 99.99995 %, was used as a carrier gas at a flow rate of 2 mL/min. The gas chromatograph was equipped with a split/splitless injection port, operating at 200 °C. Samples were injected in the splitless mode, at a column temperature of 120 °C, and the splitter was then opened after 1 min. The GC oven temperature was initially held at 120 °C for 1 min and then programmed to ramp up at 20 °C/min to 300 °C. The mass spectrometer was operated in the positive-ion electron ionization (EI) mode. Full scan data were obtained over the mass range m/z 50–600.

2.2.3. UV–Vis spectra

The UV–Vis spectra were recorded in dichloromethane (DCM) with an Agilent Technologies Cary 60 UV–Vis spectrophotometer.

2.2.4. Fluorescence spectra

Fluorescence spectra of polymers were acquired in dichloromethane (DCM) with a Cary Eclipse Fluorescence spectrofluorometer in the range 200–800 nm, and using excitation slit 5 nm and emission slit 10 nm. Excitation wavelengths were 322 nm, 322 nm, 330 nm, 320 nm, 324 nm, and 324 nm for **3a, 3b, 3c, 3d, 3e**, and **3f** respectively.

2.2.5. SEC–Molecular weight measurement

SEC–Molecular weight measurements were performed with Waters SEC chromatographic system equipped with a refractometer detector, using a guard column and three columns in series (Styragel HR2, HR4 and HR6). The analyses were performed at 35 °C and THF was used as the mobile phase at a 1 ml min^{-1} flow rate. A calibration curve was prepared with a series of polystyrenes of different molecular weight (575–3.848.000 g mol^{-1}).

2.2.6. Thermal analysis

Thermogravimetric analyses (TGA) were performed with a TGA TAQ 600 (TA Instruments) in nitrogen atmosphere with a heating gradient of 30 °C/min from 30 °C to 800 °C. Calorimetric analyses (DSC) were performed with a DSC TAQ 200 (TA Instruments) in nitrogen atmosphere with a heating gradient of 30 °C/min from −50 °C to 250 °C.

2.2.7. Elemental analysis

Elemental analysis characterization was performed with a Thermo Fisher Flash EA 1112 Series elemental analyzer (Waltham, MA, USA).

2.2.8. Synthesis procedures

2.2.8.1. 10-hexyl-10H-phenothiazine (1)[41]. The glassware was dried overnight in an oven at 150 °C. A three necked round bottom Schlenk flask (100 ml) was closed with a rubber stopper directly after extracting it from the oven. Argon was fluxed through the glassware while cooling at room temperature. In the Schlenk flask, phenothiazine (5 g, 25.1 mmol, 1 eq) was introduced and dissolved in dry DMF (50 mL) under argon atmosphere, then it was cooled to 0 °C and NaH (903 mg, 32.62 mmol, 1.5 eq) was added portion wise over 15 min and kept stirring for 1 hour. 1-Iodohexane (18 g, 38 mmol, 1.7 eq) was added to the mixture and kept stirring at RT until consumption of phenothiazine. Reaction was monitored by silica gel TLC using hexane as eluent (R_f of compound **1** = 0.4). The reaction was quenched by ice cold water and extracted three times with ethyl acetate (3 × 75 ml). Organic phase was washed three times (3 × 50 ml) with brine. After drying with anhydrous Na_2SO_4, the organic phase was filtered and evaporated under vacuum. The crude was purified by a short silica column using hexane eluent giving a yellow oil (6.319 g, 88 %).

^{1}H NMR (600 MHz, DMSO-d_6) δ ppm: 7.19 (ddd, J = 8.1, 7.3, 1.5 Hz, 2H), 7.13 (dd, J = 7.6, 1.5 Hz, 2H), 7.00 (d, J = 1.2 Hz, 2H), 6.92 (t, J =

1.1 Hz, 2H), 3.84 (t, J = 7.0 Hz, 2H), 1.65 (p, J = 6.1 Hz, 2H), 1.36 (p, J = 4.6 Hz, 2H), 1.22 (h, 4H), 0.81 (t, 3H). ^{13}C NMR (151 MHz, DMSO-d_6) δ 144.81, 127.57, 127.10, 123.63, 122.39, 115.81, 46.40, 30.82, 26.20, 25.83, 22.05, 13.82; GC-MS–-EI *m/z* calculated for $C_{18}H_{21}NS$, 283.14; found, 283 (91.17 %), 198 (100 %). Elemental analysis: calculated for $C_{18}H_{21}NS$ (283.43 a.m.u.): C 76.27 %, H 7.47 %, N 4.94 %, S 11.32 %; found: C 76.03 %, H 7.45 %, N 5.01 %, S 11.19 %.

2.2.8.2. 3,7-dibromo-10-hexyl-10H-phenothiazine (2)[42]. Compound **1** (2 g, 7.1 mmol, 1 eq) was introduced into a three-necked round bottom flask (50 ml) containing 20 mL of dichloromethane. Bromine (5.6 g, 35.3 mmol, 5 eq) was dissolved in DCM (10 mL) and added dropwise through a dropping funnel over 15 min. The reaction was stirred at room temperature until consumption of the starting material. Reaction was monitored by silica gel TLC using hexane as eluent (R_f of compound **1** = 0.4, R_f of compound **2** = 0.5). After cooling to room temperature, the reaction mixture was washed with a solution of 0.60 g KOH and 0.35 g sodium sulfite in 70 mL of water. The organic phase was separated and dried over anhydrous sodium sulfate. The solvent was evaporated under vacuum, giving a yellow oil which turned into a greenish solid on standing (2.9 g, 93 %).

^{1}H NMR (600 MHz, DMSO-d_6) δ ppm: 7.42 – 7.27 (m, 2H), 6.95 (d, J = 9.4 Hz, 2H), 3.80 (t, J = 6.9 Hz, 2H), 1.68 – 1.55 (m, Hz, 2H), 1.34 (m, J = 7.2 Hz, 2H), 1.21 – 1.15 (m, 4H), 0.77 (t, 3H). ^{13}C NMR (151 MHz, DMSO-d_6) δ 143.86, 130.40, 129.10, 125.50, 117.69, 114.03, 46.65, 30.77, 25.93, 25.70, 22.06, 13.84. GC–MS-EI *m/z* calculated for $C_{18}H_{19}Br_2NS$, 440.96; found, 444 (9.27 %), 443 (47.25 %), 442 (17.40 %), 441 (88.50 %), 440 (9.25 %), 439 (43.91), 336 (100 %) Elemental analysis: calculated for $C_{18}H_{19}Br_2NS$ (441.23 a.m.u.): C 49.00 %, H 4.34 %, N 3.17 %, S 7.27 %; found: C 49.15 %, H 4.33 %, N 3.17 %, S 7.21 %.

2.2.8.3. 3a polymer. A 20 ml MW vial was heated overnight in an oven at 150 °C and closed with a rubber stopper when extracted from the oven. Argon was flushed through the vial while cooling. The *t*-BuOK (610.37 mg, 5.44 mmol, 4 eq) was loaded into the 20 ml vial and heated with heating-gun under applied vacuum for 10 min. Argon was flushed through the vial during the following cooling. The 3,7-dibromo-10-hexyl-10H-phenothiazine (600 mg, 1.36 mmol, 1 eq), and the catalyst (IPr)Pd(allyl)Cl (15.54 mg, 0.027 mmol, 0.02 eq) were added in the vial under argon. The system was evacuated for 10 min and then filled again with argon. Dry toluene (5 ml), freshly distilled aniline (127 mg, 124 µl, 1.36 mmol, 1 eq) and a 50 mmol/L solution of 4-bromoanisole in toluene (1.53 mg, 206 µl, 8.16 µmol, 0.006 eq) were added in sequence. The vial was crimped with a septum and heated using an oil bath at 105 °C and stirred for 22 h. At the end, the mixture was left to cool and was precipitated from methanol. The crude was dissolved into dichloromethane and filtered through a short pad of silica and then washed with a 0.1 M of sodium diethyldithiocarbamate solution to remove any remaining trace of Pd. The organic phase was dried with $MgSO_4$ and concentrated under vacuum. The product was obtained from the concentrated solution by precipitation with methanol. The crude solid was extracted four times with Soxhlet with the following solvents in succession: methanol, hexane, acetone, and dichloromethane. The dichloromethane solution containing the final purified product was concentrated. The dichloromethane solution was slowly dropped into methanol (100 ml) under fast stirring and the precipitated polymer powder was recovered as solid by filtration under vacuum (100 mg, 18.3 %).

^{1}H NMR (600 MHz, THF-d_8) δ ppm: 7.30 – 6.56 (m, 11H), 4.01 – 3.75 (m, 2H), 1.80 (m, 2H), 1.46 (m, 2H), 1.39 – 1.29 (m, 4H), 1.04 – 0.80 (m, 3H). SEC (35 °C, THF): M_n = 4.9 kDa; M_w = 6.1 kDa; PDI = 1.2.

2.2.8.4. 3b polymer. **3b** polymer was prepared using the same method used for the preparation of **3a** polymer. Yield: 185 mg, 19.6 %.

^{1}H NMR (600 MHz, THF-d_8) δ ppm: 7.26 – 6.63 (m, 10H), 3.79 (m, 2H), 2.33 – 2.15 (m, 3H), 1.78 (m, 2H), 1.45 (m, 2H), 1.38 – 1.24 (m, 4H), 1.00 – 0.81 (m, 3H). SEC (35 °C, THF): M_n = 5.9 kDa; M_w = 7.7 kDa; PDI = 1.3.

2.2.8.5. 3c polymer. **3c** polymer was prepared using the same method used for the preparation of **3a** polymer. Yield: 397 mg, 40.5 %.

^{1}H NMR (600 MHz, THF-d_8) δ ppm: 7.21 – 6.22 (m, 10H), 4.13 – 3.63 (m, 5H), 1.83 (m, 2H), 1.44 (m, 2H), 1.31 (m, 4H), 0.93 – 0.78 (m, 3H). SEC (35 °C, THF): M_n = 5.0 kDa; M_w = 8.1 kDa; PDI = 1.6.

2.2.8.6. 3d polymer. **3d** polymer was prepared using the same method used for the preparation of **3a** polymer. Yield: 488 mg 43.6 %.

^{1}H NMR (600 MHz, THF-d_8) δ ppm: 7.39 – 7.16 (m, 3H), 7.02 – 6.73 (m, 12H) 3.96 – 3.74 (m, 2H), 1.78 (m, 2H), 1.45 (m, 2H), 1.37 – 1.28 (m, 2H), 0.88 (m, 3H). SEC (35 °C, THF): M_n = 2.5 kDa; M_w = 3.3 kDa; PDI = 1.3.

2.2.8.7. 3e polymer. **3e** polymer was prepared using the same method used for the preparation of **3a** polymer. Yield: 214 mg, 20.6 %.

^{1}H NMR (600 MHz, THF-d_8) δ ppm: 7.27 – 6.61 (m, 10H), 3.92 – 3.69 (m, 2H), 2.53 (m, 2H), 1.78 (m, 2H), 1.58 – 1.49 (m, 2H), 1.45 (m, 2H), 1.38 – 1.28 (m, 6H), 0.94 – 84 (t, 3H). SEC (35 °C, THF): M_n = 5.6 kDa; M_w = 7.9 kDa; PDI = 1.4.

2.2.8.8. 3f polymer. **3f** polymer was prepared using the same method used for the preparation of **3a** polymer. Yield: 355 mg, 37.3 %.

^{1}H NMR (600 MHz, THF-d_8) δ ppm: 7.34 – 6.63 (m, 10H), 4.01 – 3.74 (s, 2H), 1.78 (m, 2H), 1.45 (m, 2H), 1.36 – 1.29 (m, 4H), 0.93 – 85 (s, 3H). SEC (35 °C, THF): M_n = 4.3 kDa; M_w = 5.9 kDa; PDI = 1.4.

3. Results and discussion

3.1. Synthesis

In this study, we aimed to synthesize a novel family of polymers using Buchwald-Hartwig coupling reaction. The Buchwald-Hartwig amination process facilitates the formation of nitrogen-carbon bonds when an aryl halide reacts with a primary or secondary amine, employing a palladium catalyst and base. By employing selected commercially available low-cost anilines (see Scheme 1) in the reaction with 3,7-dibromo-10-hexyl-10H-phenothiazine **2**, we achieved a straightforward work-up process, minimizing time-consuming purification steps. The reaction was completed within 24 h, and to streamline the process, 0.01 equivalents of 4-bromoanisole were added to terminate end amino groups. The groups attached were chosen to investigate the influence of electron-withdrawing and electron-donating units on the molecular weights, optical properties, thermal stability, electrochemical properties of final polymers. The yields of polymers syntheses were 18.3, 19.6, 40.0, 43.6, 20.6, 37.3 % for **3a, 3b, 3c, 3d, 3e**, and **3f** respectively.

3.2. Characterization

3.2.1. Molecular weight measurement by SEC

The weight average molecular weight (M_w) values of all polymers ranged from 3 to 8 kDa (Table 1), indicating their suitability for enhancing device stability by protecting the perovskite active layer against degradation [24]. The obtained polymers exhibited relatively low polydispersity values ranging from 1.2 to 1.6, indicating their homogeneous nature.

3.2.2. Spectroscopic characterization

The polymeric materials **3a-f** were characterized using UV–vis and fluorescence spectroscopies (Figs. 1 and 2, and Table 2). The UV–vis spectra showed consistent patterns across all the polymers, with a maximum absorption peak ranging from 263 to 269 nm. Additionally, a

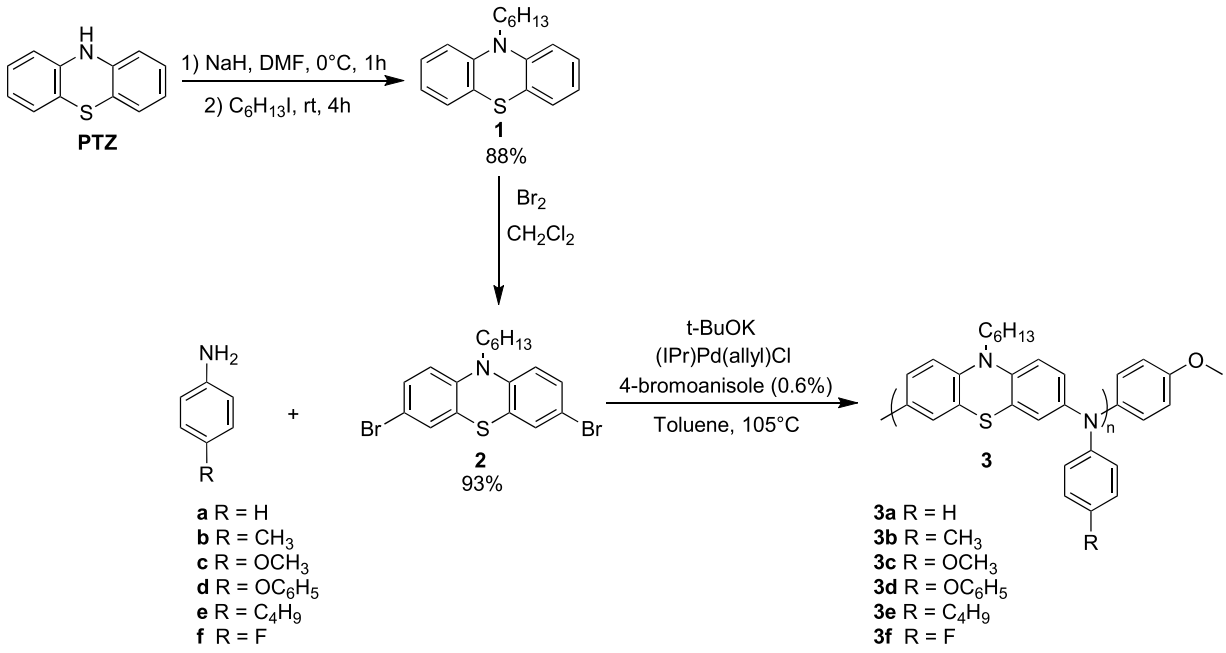

Scheme 1. Synthetic route for the polymeric materials by Buchwald-Hartwig coupling.

Table 1
Molecular weight measurement by SEC.

HTM	R	M_n[a] (kDa)	M_w[b] (kDa)	PDI[c]
3a	H	4.9	6.1	1.2
3b	CH_3	5.9	7.7	1.3
3c	OCH_3	5.0	8.1	1.6
3d	OC_6H_5	2.5	3.3	1.3
3e	C_4H_9	5.6	7.9	1.4
3f	F	4.3	5.9	1.4

[a] Average molecular weight in number.
[b] Average molecular weight in weight.
[c] Polydispersity Index (M_w/M_n).

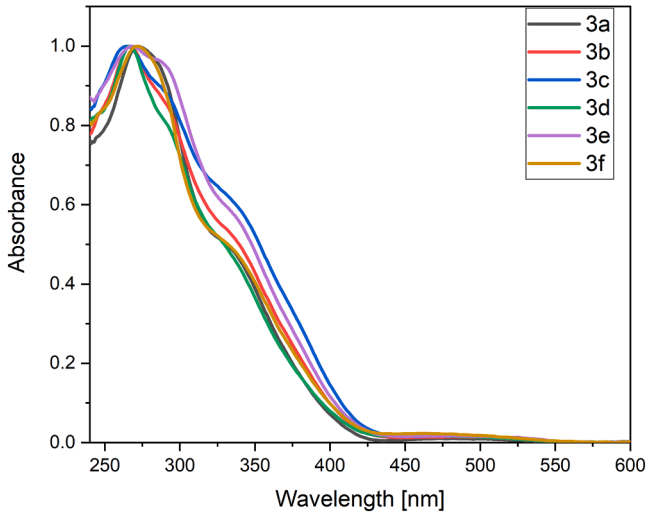

Fig. 1. UV–vis spectra of polymeric materials.

shoulder peak around 340 nm was observed, indicating their transparency in the visible region. Notably, the absorption occurred primarily in the UV region below 450 nm, suggesting their potential for efficient light absorption while allowing for transparency in the visible spectrum.

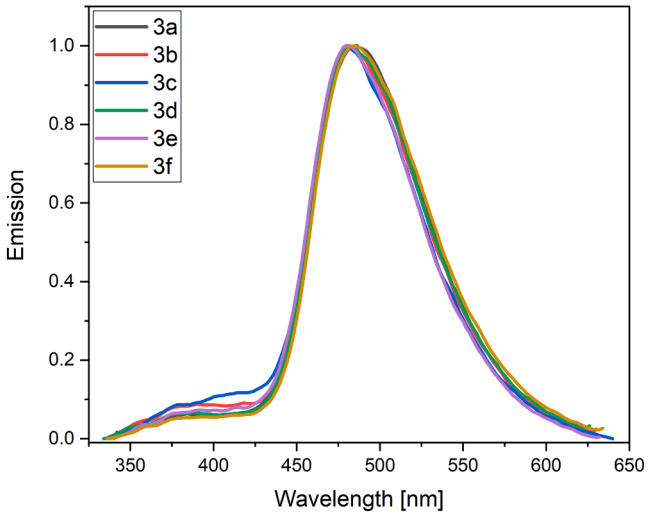

Fig. 2. Fluorescence spectra of polymeric materials.

Table 2
Optical, electrochemical and thermal characterization of the polymeric HTMs.

HTM	λ_{max} (nm)	λ_{onset} (nm)	λ_{em} (nm)	B_g (eV)	T_{stab} (°C)	T_g (°C)
3a	269	418	480	2.97	372	111.97
3b	266	430	480	2.88	373	117.91
3c	263	408	480	3.04	366	133.29
3d	266	415	480	2.99	362	119.61
3e	263	402	480	3.08	380	99.80
3f	269	422	485	2.94	376	109.34

Besides, the introduction of an electron-donating group at the para position of the aniline unit resulted in a slight blue shift in the absorption maximum. The absorption peaks for **3b, 3c, 3d**, and **3e** were measured at 266 nm, 263 nm, 266 nm, and 263 nm, respectively, compared to **3a** with a peak at 269 nm using the simple aniline unit. The F substituent (**3f**) did not show any influence on the absorption with respect the unsubstituted aniline, **3a**. Otherwise, the presence of electron-donating

units attached to the aniline unit led to a red shift in the shoulder peak at 330 nm for **3a**, with values of 335 nm, 338 nm, and 338 nm observed for **3b, 3c**, and **3e**, respectively. For **3d**, and **3f** the shoulder peak intensity was reduced. For **3f**, the spectrum was identical to **3a**. These observations agree with the expected conjugation disruption behavior of the triarylamine through its nitrogen atom. Regarding emission spectroscopy, the polymers exhibited similar behavior, displaying emission peaks within the range of 480–484 nm.

The crossing point of the UV–vis and emission spectra is normally taken as the minimum band-gap (B_g, see Table 2) for a material involved in organic electronics applications [24]. The B_g values obtained for the polymers **3a-f** agree with the transparence of those polymers towards visible light.

3.2.3. *Thermal stability through TGA and DSC*

The thermal stability of the polymers **3a-3f** was evaluated and found to be favorable (Table 2 and Fig. 3). As the general structure of the polymer is consistent across all samples, it is reasonable to expect similar thermal stability values, primarily influenced by the stability of the polymeric backbone. Nonetheless, slight variations in thermal stability were observed, likely attributable to the substituent on the para position of the aniline moiety. The obtained data revealed that the unsubstituted polymer (**3a**, $R = H$) and the polymers substituted with alkyl groups and electron acceptors (**3b**, $R = CH_3$, **3e**, $R = C_4H_9$, **3f**, $R = F$) exhibited higher stability temperatures, ranging between 372 and 380 °C. In contrast, the polymers substituted with strong electron-donor groups (**3c**, $R = OCH_3$, and **3d**, $R = OC_6H_5$) displayed slightly lower stability (362 and 366 °C, respectively), which may be attributed to the presence of the ether group. Nevertheless, overall, the polymers demonstrated very good stability, making them suitable for usual thermal processing (around 150 °C) for the fabrication of organic electronics [43].

The DSC analysis on the polymers demonstrated the presence of glass transitions, as depicted in Fig. 4 and summarized in Table 2. The observation of glass transitions is highly relevant, considering the well-established significance of this phenomenon in the field of molecular electronics and semiconductors [44]. The glass transition temperature is a critical processing parameter that governs the kinetics of molecular organization of polymer semiconductors during solidification. The organic semiconductor remains stable in the solid film structure until the glass transition temperature is reached. Moreover, stiffness is an indication of strong packing while remaining in the amorphous state, where polymer chains are in close proximity to each other, facilitating charge transfer and hole transport in the case of p-type polymers [45]. The glass transition temperatures (T_g) for **3a** and **3b** were observed at 111.97 °C and 117.91 °C, respectively, demonstrating a significant difference in stiffness between the two polymers. This disparity arises from the

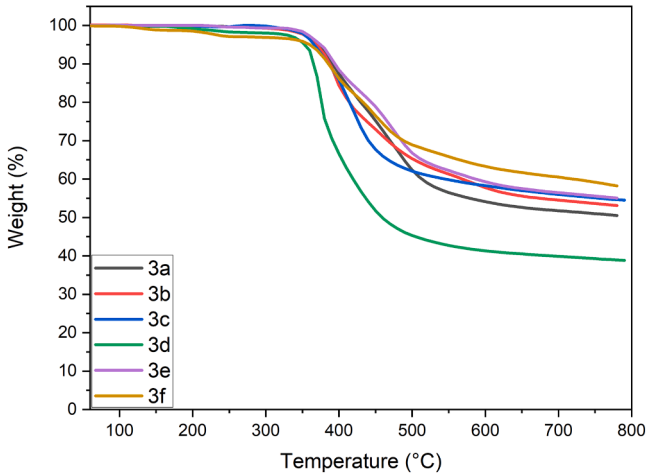

Fig. 3. TGA plots of the polymers.

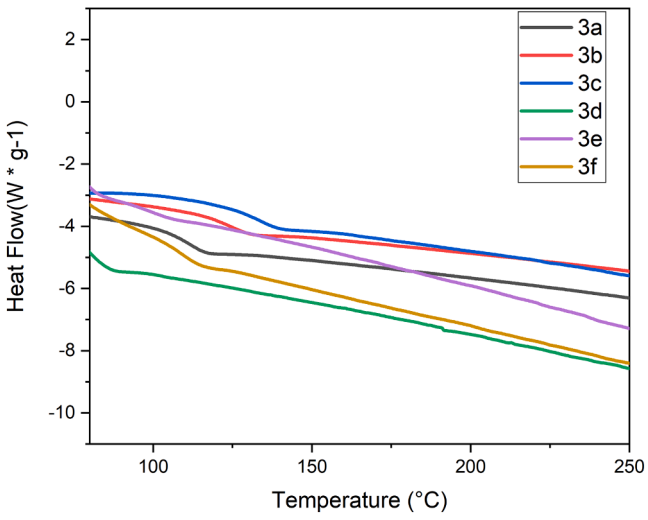

Fig. 4. DSC plots of the second heating cycle of the polymers.

presence of a methyl group in the para position of the pendant phenyl group ($R = H$ for **3a** and $R = CH_3$ for **3b**). For **3e** ($R = C_4H_9$), the glass transition is less pronounced, occurring at a lower temperature of 99.80 °C. This can be attributed to the steric hindrance caused by the butyl chain, which largely hampers polymer chain packing. Polymer **3c** exhibited a high T_g of 133.29 °C, indicating high packing and stiffness, likely due to the presence of oxygen, which can interact with portions of the polymer chain carrying a partial positive charge. Conversely, the effect is less pronounced in polymer **3d**, where the size of the benzene ring in the phenoxy group ($R = OC_6H_5$) creates greater distance between polymer chains. In summary, these materials maintain their solid phase structure in the film at around 109 °C or higher temperature, except for polymer **3e** ($R = C_4H_9$).

4. Conclusion

The synthesized polymers **(3a-3f)** have a good potential as transparent semiconductors in organic electronics. They are very appealing for large-scale production due to their simple purification procedure and cost-effective synthesis using a relatively inexpensive starting material such as phenothiazine and anilines. When exposed to high temperatures, these polymers maintain their structural integrity and amorphous structure with very good thermal stability on a reasonably large temperature range. They show high transparency and wide band gap. Overall, these properties place the here reported polymers as adaptable contenders for various transparent organic electronics applications, providing a path to the creation of scalable and effective electronic devices.

CRediT authorship contribution statement

Mohamed M.H. Desoky: Conceptualization, Investigation, Methodology, Writing – original draft. **Federico Cruciani:** Investigation. **Pierluigi Quagliotto:** Conceptualization, Funding acquisition, Investigation, Methodology, Writing – review & editing. **Guido Viscardi:** Funding acquisition, Writing – review & editing.

Declaration of competing interest

The authors declare that they have no known competing financial interests or personal relationships that could have appeared to influence the work reported in this paper.

Data availability

Data will be made available on request.

Acknowledgment

The authors gratefully acknowledge the support provided by the Ministry of Education, University and Research in of Italy (MUR) for funding the Ph.D. of Dr. M.M.H. Desoky. This work was also supported by the Italian Ministry of Environment and Energy Security in the framework of the Operating Agreement with ENEA for Research on the Electric System. The authors acknowledge support from the project CH4.0 under the MUR program "Dipartimenti di Eccellenza 2023-2027" (CUP D13C2200352001).

Supplementary materials

Supplementary material associated with this article can be found, in the online version, at doi:10.1016/j.molstruc.2024.137635.

References

[1] T. Magrini, F. Bouville, A. Lauria, H.L. Ferrand, T.P. Niebel, A.R. Studart, Transparent and tough bulk composites inspired by nacre, Nat. Commun. 10 (1) (2019) 2794, https://doi.org/10.1038/s41467-019-10829-2.
[2] Z.J. Silva, C.R. Valenta, G.D. Durgin, Optically transparent antennas: a survey of transparent microwave conductor performance and applications, IEEE Antennas Propag. Mag. 63 (1) (2021) 27–39, https://doi.org/10.1109/map.2020.2988526.
[3] V.-I. Ungureanu, R.-C. Miclea, A. Korodi, I. Silea, A novel approach against sun glare to enhance driver safety, Appl. Sci. 10 (9) (2020) 3032, https://doi.org/10.3390/app10093032.
[4] D.Y. Shin, E.H. Park, K.H. Kim, Moire-fringeless transparent conductive films with a random serpentine network of medium-field electrospun, chemically annealed silver microfibres, Sci. Rep. 9 (1) (2019) 11226, https://doi.org/10.1038/s41598-019-47779-0.
[5] T. Yamazato, S. Haruyama, Image sensor based visible light communication and its application to pose, position, and range estimations, IEICE Trans. Commun. E97 (B (9)) (2014) 1759–1765, https://doi.org/10.1587/transcom.E97.B.1759.
[6] H.J. Song, M.H. Seo, K.W. Choi, M.S. Jo, J.Y. Yoo, J.B. Yoon, High-performance copper oxide visible-light photodetector via grain-structure model, Sci. Rep. 9 (1) (2019) 7334, https://doi.org/10.1038/s41598-019-43667-9.
[7] B.J. Kim, N.K. Cho, S. Park, S. Jeong, D. Jeon, Y. Kang, T. Kim, Y.S. Kim, I.K. Han, S.J. Kang, Highly transparent phototransistor based on quantum-dots and ZnO bilayers for optical logic gate operation in visible-light, RSC Adv. 10 (28) (2020) 16404–16414, https://doi.org/10.1039/d0ra01756f.
[8] F.M. Wu, C.T. Lin, C.C. Wei, C.W. Chen, Z.Y. Chen, H.T. Huang, C. Sien, Performance comparison of OFDM Signal and CAP signal over high capacity RGB-LED-based WDM visible light communication, IEEE Photonics J. 5 (4) (2013) 7901507, https://doi.org/10.1109/jphot.2013.2271637.
[9] D.H. Sin, S.H. Kim, J. Lee, H. Lee, Modification of electrode interface with fullerene-based self-assembled monolayer for high-performance organic optoelectronic devices, Micromachines (Basel) 13 (10) (2022) 1613, https://doi.org/10.3390/mi13101613.
[10] S. Fratini, M. Nikolka, A. Salleo, G. Schweicher, H. Sirringhaus, Charge transport in high-mobility conjugated polymers and molecular semiconductors, Nat. Mater. 19 (5) (2020) 491–502, https://doi.org/10.1038/s41563-020-0647-2.
[11] H. Tanaka, T. Yasuda, K. Fujita, T. Tsutsui, Transparent image sensors using an organic multilayer photodiode, Adv. Mater. 18 (17) (2006) 2230–2233, https://doi.org/10.1002/adma.200600163.
[12] R. Meng, Q. Jiang, D. Liu, Balancing efficiency and transparency in organic transparent photovoltaics, npj Flexible Electron. 6 (1) (2022), https://doi.org/10.1038/s41528-022-00173-9.
[13] Z. Pei, H.-C. Lai, J.-Y. Wang, W.-H. Chiang, C.-H. Chen, High-responsivity and high-sensitivity graphene dots/a-IGZO thin-film phototransistor, IEEE Electron. Dev. Lett. 36 (1) (2015) 44–46, https://doi.org/10.1109/led.2014.2368773.
[14] S.W. Shin, K.H. Lee, J.S. Park, S.J. Kang, Highly transparent, visible-light photodetector based on oxide semiconductors and quantum dots, ACS Appl. Mater. Interfaces 7 (35) (2015) 19666–19671, https://doi.org/10.1021/acsami.5b04683.
[15] B.J. Kim, J.H. Jeong, E.Y. Jung, T.Y. Kim, S. Park, J.A. Hong, K.M. Lee, W. Jeon, Y. Park, S.J. Kang, A visible-light phototransistor based on the heterostructure of ZnO and TiO(2) with trap-assisted photocurrent generation, RSC Adv. 11 (20) (2021) 12051–12057, https://doi.org/10.1039/d1ra00801c.
[16] H. Shin, D.Y. Kim, Rotating gate-driven solution-processed triboelectric transistors, Sensors 22 (9) (2022) 3309, https://doi.org/10.3390/s22093309.
[17] M. Xu, M. Nakamura, K. Kudo, Thickness dependence of mobility of pentacene planar bottom-contact organic thin-film transistors, Thin Solid Films 516 (9) (2008) 2776–2778, https://doi.org/10.1016/j.tsf.2007.04.115.
[18] D. Gupta, Y. Hong, Understanding the effect of semiconductor thickness on device characteristics in organic thin film transistors by way of two-dimensional simulations, Org. Electron. 11 (1) (2010) 127–136, https://doi.org/10.1016/j.orgel.2009.10.009.
[19] Q. Li, J. van de Groep, Y. Wang, P.G. Kik, M.L. Brongersma, Transparent multispectral photodetectors mimicking the human visual system, Nat. Commun. 10 (1) (2019) 4982, https://doi.org/10.1038/s41467-019-12899-8.
[20] C.K. Chiang, Y.W. Park, A.J. Heeger, H. Shirakawa, E.J. Louis, A.G. MacDiarmid, Conducting polymers: halogen doped polyacetylene, J. Chem. Phys. 69 (11) (1978) 5098–5104, https://doi.org/10.1063/1.436503.
[21] H.F. Haneef, A.M. Zeidell, O.D. Jurchescu, Charge carrier traps in organic semiconductors: a review on the underlying physics and impact on electronic devices, J. Mater. Chem. C 8 (3) (2020) 759–787, https://doi.org/10.1039/c9tc05695e.
[22] A. Isakova, P.D. Topham, Polymer strategies in perovskite solar cells, J. Polym. Sci. Part B 55 (7) (2017) 549–568, https://doi.org/10.1002/polb.24301.
[23] W. Zhou, Z. Wen, P. Gao, Less is more: dopant-free hole transporting materials for high-efficiency perovskite solar cells, Adv. Energy Mater. 8 (9) (2018) 1702512, https://doi.org/10.1002/aenm.201702512.
[24] N. Yaghoobi Nia, M. Bonomo, M. Zendehdel, E. Lamanna, M.M.H. Desoky, B. Paci, F. Zurlo, A. Generosi, C. Barolo, G. Viscardi, P. Quagliotto, A. Di Carlo, Impact of P3HT regioregularity and molecular weight on the efficiency and stability of perovskite solar cells, ACS Sustain. Chem. Eng. 9 (14) (2021) 5061–5073, https://doi.org/10.1021/acssuschemeng.0c09015.
[25] H. Bronstein, C.B. Nielsen, B.C. Schroeder, I. McCulloch, The role of chemical design in the performance of organic semiconductors, Nat. Rev. Chem. 4 (2) (2020) 66–77, https://doi.org/10.1038/s41570-019-0152-9.
[26] A.D. Scaccabarozzi, A. Basu, F. Anies, J. Liu, O. Zapata-Arteaga, R. Warren, Y. Firdaus, M.I. Nugraha, Y. Lin, M. Campoy-Quiles, N. Koch, C. Muller, L. Tsetseris, M. Heeney, T.D. Anthopoulos, Doping approaches for organic semiconductors, Chem. Rev. 122 (4) (2022) 4420–4492, https://doi.org/10.1021/acs.chemrev.1c00581.
[27] S. Revoju, A. Matuhina, L. Canil, H. Salonen, A. Hiltunen, A. Abate, P. Vivo, Structure-induced optoelectronic properties of phenothiazine-based materials, J. Mater. Chem. C 8 (44) (2020) 15486–15506, https://doi.org/10.1039/d0tc03421e.
[28] R. Duesing, G. Tapolsky, T.J. Meyer, Long-range, light-induced redox separation across a ligand bridge, J. Am. Chem. Soc. 112 (13) (2002) 5378–5379, https://doi.org/10.1021/ja00169a071.
[29] T.L. Mako, J.M. Racicot, M. Levine, Supramolecular luminescent sensors, Chem. Rev. 119 (1) (2019) 322–477, https://doi.org/10.1021/acs.chemrev.8b00260.
[30] J. Daub, R. Engl, J. Kurzawa, S.E. Miller, S. Schneider, A. Stockmann, M. R. Wasielewski, Competition between conformational relaxation and intramolecular electron transfer within phenothiazine−pyrene dyads, J. Phys. Chem. A 105 (23) (2001) 5655–5665, https://doi.org/10.1021/jp0037293.
[31] X.H. Zhang, H.K. Seon, S.L. In, J.G. Chun, S.I. Yang, K.H. Ahn, Synthesis, photophysical and electrochemical properties of novel conjugated donor-acceptor molecules based on phenothiazine and benzimidazole, Bull. Korean Chem. Soc. 28 (8) (2007) 1389–1395, https://doi.org/10.5012/bkcs.2007.28.8.1389.
[32] I.J. Al-Busaidi, A. Haque, N.K. Al Rasbi, M.S. Khan, Phenothiazine-based derivatives for optoelectronic applications: a review, Synth. Met. 257 (2019) 116189, https://doi.org/10.1016/j.synthmet.2019.116189.
[33] Y.S. Han, S.D. Kim, L.S. Park, D.U. Kim, Y. Kwon, Synthesis of conjugated copolymers containing phenothiazinylene vinylene moieties and their electrooptic properties, J. Polym. Sci., Part A: Polym. Chem. 41 (16) (2003) 2502–2511, https://doi.org/10.1002/pola.10793.
[34] L.M. Moshurchak, C. Buhrmester, J.R. Dahn, Triphenylamines as a class of redox shuttle molecules for the overcharge protection of lithium-ion cells, J. Electrochem. Soc. 155 (2) (2008), https://doi.org/10.1149/1.2816229.
[35] P.Y. Gu, N. Wang, A. Wu, Z. Wang, M. Tian, Z. Fu, X.W. Sun, Q. Zhang, An azaacene derivative as promising electron-transport layer for inverted perovskite solar cells, Chem. Asian J. 11 (15) (2016) 2135–2138, https://doi.org/10.1002/asia.201600856.
[36] R. Dorel, C.P. Grugel, A.M. Haydl, The Buchwald–Hartwig amination after 25years, Angew. Chem. 131 (48) (2019) 17276–17287, https://doi.org/10.1002/ange.201904795.
[37] M. Fitzner, G. Wuitschik, R.J. Koller, J.M. Adam, T. Schindler, J.L. Reymond, What can reaction databases teach us about Buchwald-Hartwig cross-couplings? Chem. Sci. 11 (48) (2020) 13085–13093, https://doi.org/10.1039/d0sc04074f.
[38] S.W. Goldstein, A. Bill, J. Dhuguru, O. Ghoneim, Nucleophilic aromatic substitution—addition and identification of an amine, J. Chem. Educ. 94 (9) (2017) 1388–1390, https://doi.org/10.1021/acs.jchemed.6b00680.
[39] Q. Yang, Y. Zhao, D. Ma, Cu-mediated Ullmann-type cross-coupling and industrial applications in route design, process development, and scale-up of pharmaceutical and agrochemical processes, Org. Process Res. Dev. 26 (6) (2022) 1690–1750, https://doi.org/10.1021/acs.oprd.2c00050.
[40] R.S. Sprick, M. Hoyos, J.J. Morrison, I.M. Grace, C. Lambert, O. Navarro, M. L. Turner, Triarylamine polymers of bridged phenylenes by (N-heterocyclic carbene)-palladium catalysed C–N coupling, J. Mater. Chem. C 1 (20) (2013) 3327–3336, https://doi.org/10.1039/c3tc30368c.
[41] C. Yin, H. Zhu, C. Xie, L. Zhang, P. Chen, Q. Fan, W. Huang, K. Pu, Organic nanoprobe cocktails for multilocal and multicolor fluorescence imaging of reactive oxygen species, Adv. Funct. Mater. 27 (23) (2017), https://doi.org/10.1002/adfm.201700493.
[42] Y.S. Yang, H.D. Kim, J.-H. Ryu, K.K. Kim, S.S. Park, K.-S. Ahn, J.H. Kim, Effects of anchoring groups in multi-anchoring organic dyes with thiophene bridge for dye-

sensitized solar cells, Synth. Met. 161 (9–10) (2011) 850–855, https://doi.org/10.1016/j.synthmet.2011.02.012.
[43] S.H. Reddy, F. Di Giacomo, A. Di Carlo, Low-temperature-processed stable perovskite solar cells and modules: a comprehensive review, Adv. Energy Mater. 12 (13) (2022), https://doi.org/10.1002/aenm.202103534.
[44] C. Müller, On the glass transition of polymer semiconductors and its impact on polymer solar cell stability, Chem. Mater. 27 (8) (2015) 2740–2754, https://doi.org/10.1021/acs.chemmater.5b00024.
[45] S. Prodhan, J. Qiu, M. Ricci, O.M. Roscioni, L. Wang, D. Beljonne, Design rules to maximize charge-carrier mobility along conjugated polymer chains, J. Phys. Chem. Lett. 11 (16) (2020) 6519–6525, https://doi.org/10.1021/acs.jpclett.0c01793.